Reservoir Lithology Determination by Hidden Markov Random Fields Based on a Gaussian Mixture Model

Feng, Runhai; Luthi, Stefan M.; Gisolf, Dries; Angerer, Erika

DOI
10.1109/TGRS.2018.2841059

Publication date
2018

Document Version
Accepted author manuscript

Published in
IEEE Transactions on Geoscience and Remote Sensing

Citation (APA)
Feng, R., Luthi, S. M., Gisolf, D., & Angerer, E. (2018). Reservoir Lithology Determination by Hidden Markov Random Fields Based on a Gaussian Mixture Model. *IEEE Transactions on Geoscience and Remote Sensing*, *56*(11), 6663-6673. https://doi.org/10.1109/TGRS.2018.2841059

Reservoir Lithology Determination by Hidden Markov Random Fields Based on a Gaussian Mixture Model

Runhai Feng, Stefan M. Luthi, Dries Gisolf, and Erika Angerer

***Abstract*— In this paper, geological prior information is incorporated in the classification of reservoir lithologies after the adoption of Markov random fields (MRFs). The prediction of hidden lithologies is based on measured observations, such as seismic inversion results, which are associated with the latent categorical variables, based on the assumption of Gaussian distributions. Compared with other statistical methods, such as the Gaussian mixture model or *k*-Means, which do not take spatial relationships into account, the hidden MRFs approach can connect the same or similar lithologies horizontally while ensuring a geologically reasonable vertical ordering. It is, therefore, able to exclude randomly appearing lithologies caused by errors in the inversion. The prior information consists of a Gibbs distribution function and transition probability matrices. The Gibbs distribution connects the same or similar lithologies internally, which does not need a geological definition from the outside. The transition matrices provide preferential transitions between different lithologies, and an estimation of them implicitly depends on the depositional environments and juxtaposition rules between different lithologies. Analog cross sections from the subsurface or outcrop studies can contribute to the construction of these matrices by a simple counting procedure.**

***Index Terms*— Hidden Markov random fields (HMRFs), lithology determination, seismic inversion, transition matrix.**

I. Introduction

THE classification of lithologies is an essential step in reservoir characterization and in the building of a static reservoir model. The definition, the number, and the types of lithologies can be provided by geologists. The preliminary analysis of well-log data will identify various lithologies, and most of the time, the number of lithologies will be kept constant afterward. Other sources of information, such as seismic data, can provide a larger areal coverage, thus overcoming the limitations provided by sparse well locations.

Inference of lithologies from seismic data is a challenging task and actually an ill-posed inverse problem, because a variety of different facies characteristics may result in identical or similar seismic responses [1]. The Bayesian concept is usually applied to mitigate this problem as applied by Mukerji *et al.* [2] and Houck [3] who identified lithology/fluid (LF) classes based on the amplitude-versus-offset (AVO) analysis. Buland and Omre [4] developed a linearized AVO inversion approach under the Bayesian framework. Subsequently, Buland *et al.* [5] proposed a fast Bayesian inversion approach for a 3-D lithology and fluid prediction from prestack data.

However, the approaches mentioned previously are point- or location-based, which means that the spatial coupling between data points is not considered. In order to address this problem, prior information can be included, in which a Markov chain or Markov random field (MRF) is applied. Eidsvik *et al.* [6] translated well-log data into geological attributes by hidden Markov chains. Larsen *et al.* [1] incorporated a stationary Markov-chain prior model to simulate vertical continuity of LF classes along the profile. Ulvmoen and Hammer [7] compared two algorithms—approximated and exact likelihood models for the inversion of lithologies and fluids in which the Markov *a priori* knowledge is incorporated in the Bayesian setting. Ulvmoen *et al.* [8], [9] adopted a profile MRF model to simulate *a priori* information of the LF classes in order to improve the resolution in the Bayesian LF inversion from prestack seismic data. Hammer *et al.* [10] inverted a vertical profile of rock properties based on seismic amplitude data in which a Markov prior process is included to guarantee that vertical dependences are honored. Other reservoir parameters, such as porosity and saturation, could also be inferred from seismic data combined with well observations as have been done by Bosch *et al.* [11].

In this paper, instead of deriving the lithologies from prestack or stacked seismic data, the efforts are geared toward the usage of inversion results in reservoir description. The elastic full-wavefield inversion scheme can provide high-resolution results, because the intrinsically nonlinear relationship between rock properties and the seismic data has been fully exploited [12]. This feature makes the approach suitable as a potential input for the reservoir characterization process.

The 3-D distribution of lithologies in the subsurface is not directly observable, or hidden, with only limited information provided by wells. However, indirect observations in the form of measurements are available that contain information on them. Hidden Markov models (HMMs) are trying to uncover

Manuscript received October 13, 2017; revised March 22, 2018; accepted May 22, 2018. This work was supported by the DELPHI Consortium. *(Corresponding author: Runhai Feng.)*

R. Feng and S. M. Luthi are with the Department of Geoscience and Engineering, Delft University of Technology, 2628 CN Delft, The Netherlands (e-mail: r.feng@tudelft.nl).

D. Gisolf is with the Department of Physics, Delft University of Technology, 2628 CJ Delft, The Netherlands.

E. Angerer is with OMV Exploration & Production, 1020 Vienna, Austria.

Color versions of one or more of the figures in this paper are available online at http://ieeexplore.ieee.org.

Digital Object Identifier 10.1109/TGRS.2018.2841059

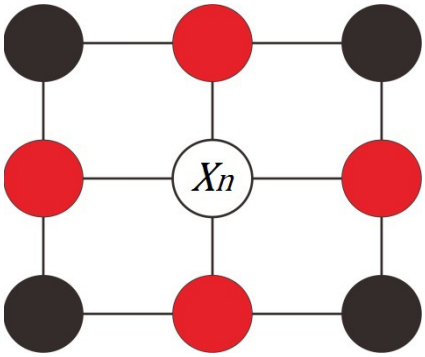

Fig. 1. Schematic view of the dependence between nodes.

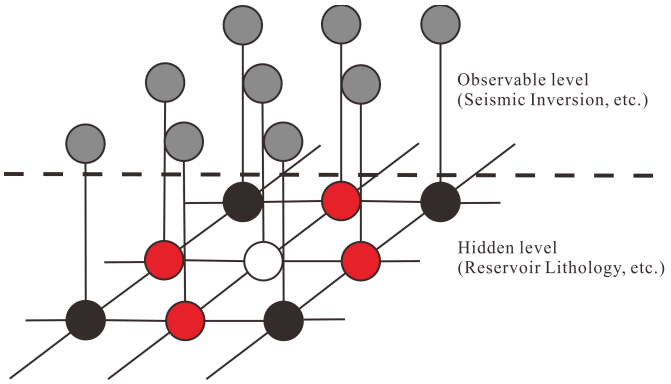

Fig. 2. HMRFs with observable and hidden levels.

these latent states under this concept but only in 1-D, i.e., the vertical direction [6], [13]. Here, we present a 2-D method, in which the horizontal prior information is also incorporated through the introduction of MRFs.

The rock properties obtained by the inversion of seismic data are assumed to be distributed according to multivariate Gaussian functions [14]. Thus, a Gaussian mixture model (GMM) is used to describe the conditional probabilities of the properties from inverted seismic data, given different lithologies [15].

In this paper, first a short introduction of the MRFs is given, and then the theory of the GMM-based hidden MRFs (GMM-HMRFs) is described. Finally, some synthetic examples and a field case study from Vienna Basin will be shown with discussions and some conclusions.

II. Markov Random Fields

First introduced by Ising [16], a MRF is an undirected graphical model and can be described by a group of random variables that possess a Markov property. This Markov property can be defined by a joint probability distribution, which is determined by a local conditional distribution. Fig. 1 illustrates this concept in which the white node is independent of all other black nodes given the red nodes.

The following equation describes the conditional distribution of X_n:

$$\Pr(X_n|X_m, m \neq n) = \Pr(X_n|X_m, m \in \varepsilon) \tag{1}$$

where X_n can take a value in the set of categorical variables, such as lithology, which is associated with the node n; ε represents the local neighborhood set of nodes that share an edge with node n in the graph.

However, it is not easy to construct the joint distribution of a MRF based on the local conditional distribution of $\Pr(X_n|X_m, m \in \varepsilon)$. The Hammersley–Clifford theorem builds the equality between the joint distribution of any MRF and a Gibbs distribution; the joint distribution of a MRF can be defined by a clique potential (see in the following) [17], [18]. A Gibbs distribution is taking the form

$$\Pr(\mathbf{X}) = \frac{1}{Z} e^{-U(\mathbf{X})} \tag{2}$$

in which

$$U(\mathbf{X}) = \sum_{c \in C} V_c(\mathbf{X}) \tag{3}$$

where $\Pr(\mathbf{X})$ is the probability distribution of random variables $\mathbf{X}$, $U(\mathbf{X})$ is the energy function, Z is the partition function, c is a clique which is a subset of nodes satisfying the demand that every node is linked to every other one, and C is the set of c; $V_c(\mathbf{X})$ can be referred as clique potential functions [19].

III. Gaussian Mixture Model-Based Hidden Markov Random Fields

Similar to HMMs [6], [20], HMRFs are also trying to uncover the categorical variables that are hidden to the observers (Fig. 2). The difference with HMMs is that the theory of 2-D MRFs is applied, instead of a vertical Markov chain, which has no limitation in 1-D (depth). That is why it is more suitable for quantifying reservoir properties in 2-D or even 3-D, since both the vertical and horizontal connections in categorical variables are considered.

In the HMRFs, the hidden level is associated with categorical variables in physical space, whereas in the observable level, the data can be obtained in statistical space. Hence, a HMRF model is defined as a stochastic process derived by a MRF whose label configuration cannot be observed directly [19]. However, a MRF could generate measurable data sets that are assumed to honor certain probability distribution functions known as the emission probability functions [19], [20].

According to the maximum a posterior criterion, in HMRFs, the purpose is to seek the states $\hat{\mathbf{X}}$ that satisfy [21], [22]

$$\hat{\mathbf{X}} = \underset{\mathbf{X}}{\operatorname{argmax}} \{\Pr(\mathbf{Y}|\mathbf{X}, \theta)\Pr(\mathbf{X})\} \tag{4}$$

where $\Pr(\mathbf{X})$ is the prior probability, which is a Gibbs distribution in (2); $\Pr(\mathbf{Y}|\mathbf{X}, \theta)$ is the likelihood probability of the observation $\mathbf{Y}$.

A typical characteristic of $\Pr(\mathbf{Y}|\mathbf{X}, \theta)$ is the conditional independence of any particular configuration of $\mathbf{X}$ [21], [22]

$$\Pr(\mathbf{Y}|\mathbf{X}, \theta) = \prod_i \Pr(Y_i|X_i, \theta_{X_i}) \tag{5}$$

$\Pr(Y_i|X_i, \theta_{X_i})(i = 1, 2, \ldots, T$; where T is the total number of data samples) is the emission distribution of observation Y_i, with parameters θ_{X_i}. Different probability functions can be applied to describe it, but to keep analytical tractability, a Gaussian assumption is made [13].

Given the observation data $\mathbf{Y}$, for a certain state X_i, which takes a value in the state space $\mathbf{S} = \{S_1, S_2, \cdots, S_N\}$, the Gaussian distribution has the following form with the means μ_j and the covariance matrices σ_j ($j = 1, 2, \ldots, N$; where N is the total number of lithologies):

$$\Pr(Y_i|X_i = S_j, \theta_j) = f(Y_i; \mu_j, \sigma_j) \tag{6}$$

where $\theta_j = (\mu_j, \sigma_j)$ which is a specified θ_{X_i} when $X_i = S_j$ and

$$f(Y_i; \mu_j, \sigma_j) = \frac{1}{\sqrt{2\pi\sigma_j^2}} \exp\left(-\frac{(Y_i - \mu_j)^2}{2\sigma_j^2}\right) \tag{7}$$

In (7), the intensity distribution of each state, or lithology to be classified, is a Gaussian distribution with the parameter sets $\theta_j = (\mu_j, \sigma_j)$. However, sometimes, it is insufficient to describe the complexity in the distribution of the observation data, especially for multimodal distributions. Thus, a GMM is more powerful than a single Gaussian function to model the complexity and can be described in the following with the parameter sets θ_j in which there are k components [15]:

$$\theta_j = \{(\mu_{j,1}, \sigma_{j,1}, \omega_{j,1}), \ldots, (\mu_{j,k}, \sigma_{j,k}, \omega_{j,k})\} \tag{8}$$

where $\omega_{j,k}$ is a mixture weight of the kth component given a specific state S_j.

Accordingly, (7) will have a weighted probability form

$$f(Y_i; \theta_j) = \sum_{n=1}^{k} \omega_{j,n} f(Y_i; \mu_{j,n}, \sigma_{j,n}) \tag{9}$$

Without the spatial correlation of $\Pr(\mathbf{X})$, (4) will become a degenerated case of HMRFs, in which the GMM is defined and can be specified fully by the histogram of the data [22]. After the incorporation of $\Pr(\mathbf{X})$ as a prior, the classification problem is then approached statistically as well as spatially.

However, the prior $\Pr(\mathbf{X})$ only considers the spatial correlation of the neighbors and tries to make the same (constant image) or similar (continuous image) prediction with the contextual constraints, and it does not need a specification of geological knowledge which can be considered as an internal prior. Thus, this is not sufficient, because some unrealistic classifications could happen, such as a water sand on top of a gas or oil sand in a given reservoir. This could be due to measurement errors or misleading neighbors because of the tendency to be the same or a similar state or lithology (Fig. 1) [13]. Therefore, a profile Markov matrix as an external prior is proposed in which another constraint on lithological transitions will be introduced.

Unlike a traditional Markov chain matrix, which is obtained by counting the transitions of lithologies in the vertical direction (depth) and normalizing afterward [23], the construction of this new profile Markov matrix is using the same procedure as the Markov chain in which the counting and normalizing in the vertical direction will be kept, while also the left and right neighbors in the lateral direction of the future state are considered [8], [9]. A detailed description of this prior matrix $P_{(:,:)}$ is provided in Appendix A.

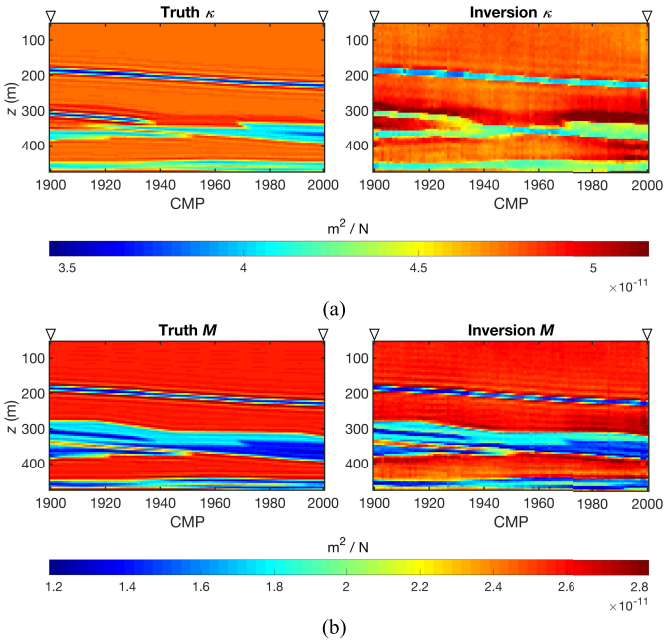

Fig. 3. True and inverted properties of a selected part from the Book Cliffs model. (a) κ. (b) M. The inverse triangle represents the location of the two well logs (CMP = 1900 and 2000).

Thus, (4) has to be reformatted in order to take matrix $P_{(:,:)}$ into account

$$\hat{\mathbf{X}} = \underset{\mathbf{X}}{\operatorname{argmax}} \{\Pr(\mathbf{Y}|\mathbf{X}, \theta)\mathbf{Pr}(\mathbf{X})P_{(:,:)}\} \tag{10}$$

In order to find an estimated $\hat{\mathbf{X}}$, (10) is invoked, in which both the states and the parameter sets in the GMM are unknown, as described previously. Furthermore, they are connected with each other. Different techniques have been introduced to solve this problem, in which the expectation–maximization (EM) method is the one most widely used [22]. The strategy in the EM approach is as follows. Given the current estimated θ, predict the hidden variables $\hat{\mathbf{X}}$; then, θ can be updated by maximizing the expectation of the complete-data likelihood function $\mathrm{E}[\Pr(\mathbf{X}, \mathbf{Y}|\theta)P_{(:,:)}]$ [19], [22]. This process will be iterated until certain conditions are met. For the mathematical details, please refer to Zhang *et al.* [22].

IV. Book Cliffs Example

The first example for applying the approach is the synthetic Book Cliffs model created by Feng *et al.* [24] in which more details have been added and more differentiation is put on the potential reservoir lithologies than in the original [25]. As a test, only a subset of the whole 2-D section has been selected, and Fig. 3 shows the true and inverted properties in terms of κ and M ($\kappa = 1/K$, with K being the bulk modulus; $M = 1/\mu$, with μ being the shear modulus).

The quality of inversion results is quite good when compared with the truth, since most geometries have been recovered correctly, as well as the properties, which is due to the fact that the nonlinear relationship between rock properties and seismic data has been fully exploited [12]. Observations from wells are needed for inferring the prior

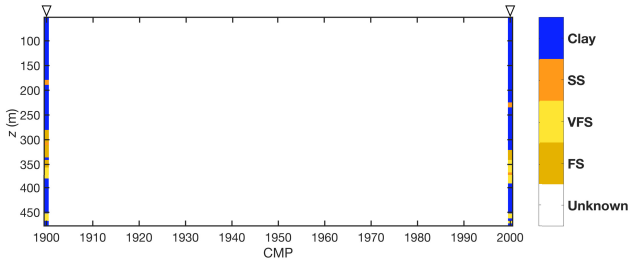

Fig. 4. Two pseudowells at CMP = 1900 and 2000 as indicated by the inverse triangle. Lithologies are known at the well locations with FS, VFS, SS, and clay.

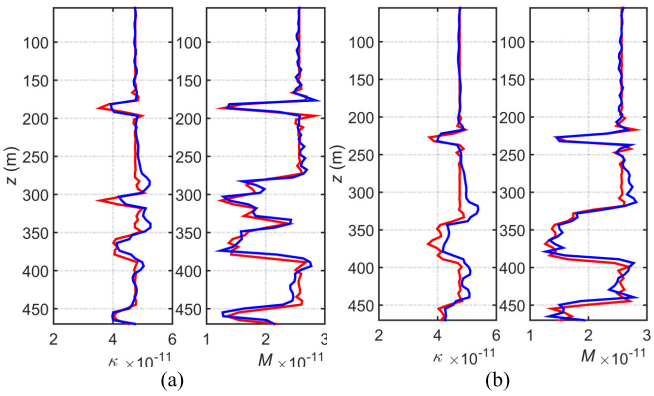

Fig. 5. True (red curves) and inverted (blue curves) properties at (a) CMP = 1900 and (b) CMP = 2000. Note that the values in the wells have been upscaled to the seismic grid interval.

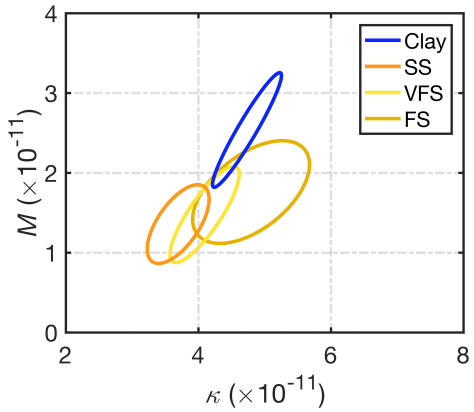

Fig. 6. 90% confidence regions of the bivariate Gaussian likelihood model for the distribution of each lithology.

Markov models [8], [9] as well as for building the lithological templates. As a starting point of the classification process, two pseudowells have been "drilled" at the leftmost and rightmost locations of the selected section (CMP = 1900 and 2000) (Fig. 4).

The true and inverted properties at the well locations can be seen in Fig. 5. Fig. 6 shows 90% confidence regions of the Bivariate Gaussian likelihood model in terms of κ and M.

From Fig. 6, it can be seen that there are some overlapping areas between different lithologies, especially for siltstone (SS) and very fine-grained sandstone (VFS), which makes the

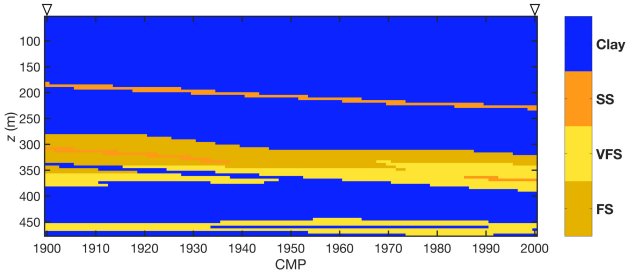

Fig. 7. Subsurface cross section in terms of lithologies.

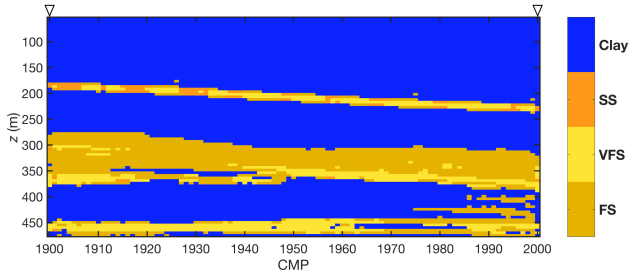

Fig. 8. Starting model in terms of lithologies (MCC = 0.4234).

differentiation difficult when only the property values are considered. Therefore, the Gaussian likelihood model (Fig. 6) is adopted which is the emission probability of properties given a specific lithology (5) [20]. However, in contrast to other statistical methods, such as GMM or k-Means [26], two additional parameter sets are introduced in GMM-HMRFs: the Gibbs prior distribution and the profile Markov matrix. These ensure that the geological information is implicitly incorporated during the classification process. Fig. 7 displays the cross-sectional truth in the subsurface. The starting model of the classification is shown in Fig. 8, which is derived from a noniterative histogram-based statistical approach with the two "drilled" wells as lithological templates and inversion results as inputs (Figs. 3–6). In order to measure the quality of the lithological prediction, the Matthew's correlation coefficient (MCC) is adopted for which the value range is $[-1\ 1]$, where 1 means a perfect prediction and -1 represents the worst result [27].

Since only the inverted property values are used, there is no spatial correlation between the sample points, which makes the prediction unreliable in the form of randomly appearing lithologies, particularly at the layer boundaries. Subsequently the GMM methodology is applied with the lithological distributions in Fig. 8 as inputs. By contrast with the simple histogram-based and noniterative approach used in Fig. 8, the GMM clusters sample points into different groups (lithologies), by applying an iterative procedure called EM, as discussed previously.

The EM algorithm finds the maximum likelihood estimates of parameters in probabilistic models in the presence of missing data, which in this context means that the lithologies are unknown [13]. An iterative scheme is performed in which the expectation step calculates the probability of every sample

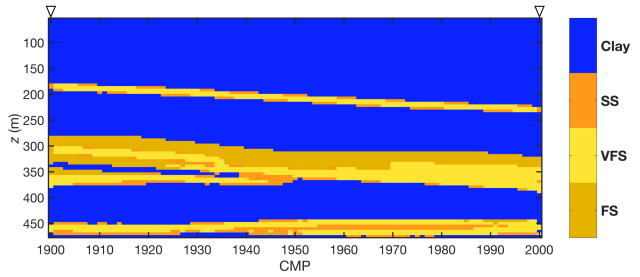

Fig. 9. Result of GMM with the starting model shown in Fig. 8 (MCC = 0.5245).

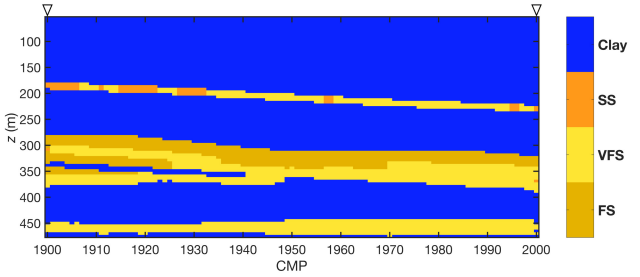

Fig. 10. Result of GMM-HMRFs incorporated with the Gibbs prior only (MCC = 0.6600).

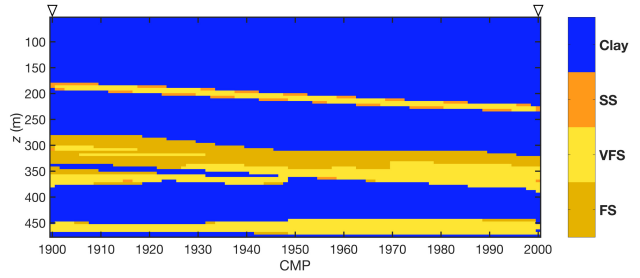

Fig. 11. Result of GMM-HMRFs incorporated with the Markov matrix only (MCC = 0.6417).

point belonging to each lithology, whereas in the maximization step, it maximizes the means and covariance matrices according to the probabilities computed in the expectation step. As in [28], the spatial correlation is ignored in the estimation of these parameters here in which some random states or lithologies still occur, although the result in Fig. 9 is improved compared with the initial one in Fig. 8.

In order to test the different roles of the prior information, i.e., the Gibbs function (2) and the Markov matrix (Appendix A), results incorporated with the prior information separately are shown (Figs. 10 and 11). With only the Gibbs prior used (Fig. 10), some lithologies are better connected than with the GMM (Fig. 9). However, some random lithologies still exist such as the SS in the VFS layer in the upper part and the FS (fine-grained sandstone) in the lower-middle area, which has been separated because of locally connected VFS at the depths between 300m and 350m and CMPs between 1925 and 1940.

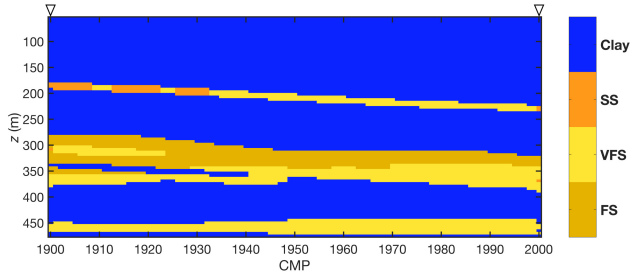

Fig. 12. Result of GMM-HMRFs incorporated with both prior information (MCC = 0.7034).

With only the Markov matrix used, the distribution of lithologies is preferential in the horizontal direction (Fig. 11), since the transition has been governed by the left and right neighbors, demonstrated as larger values, that provides information on the lateral continuity or is under the consideration of layered formations (Appendix A) [29]. However, these matrices have to be modified in order to simulate transitions in a given reservoir which will be discussed in the real case study in the following.

By applying both prior information, the spatial correlation is considered in the vertical and horizontal directions. Compared with the result by the GMM (Fig. 9) and others with either one of the prior information incorporated (Figs. 10 and 11), the classified lithologies (Fig. 12) are distributed more orderly and closer to the truth (Fig. 7), as well as shown by an increase of MCC values [30].

V. Real Case Study in the Vienna Basin

In order to further test the ability of the proposed GMM-HMRFs, a real field data set from the Vienna Basin is used. Vintages of 3-D seismic surveys acquired in different years have been merged into a single data set, Vienna Basin Super Merge, which are used as inputs for the nonlinear elastic full-wavefield inversion scheme [12]. The inverted rock properties from the seismic data are then used as inputs for the lithology prediction as illustrated previously.

A single cross section of inverted rock properties (κ and M) has been selected from the available data set, which is traversed by a logged well in the middle (Fig. 13).

Due to problems in the preprocessing phase, or fault cut-outs, or both, the inversion result is of suboptimal quality, even though in the upper part of the well, the match is quite reasonable (Fig. 14). Fig. 15 shows the properties' confidence regions of three groups of lithologies.

In order to perform the new classification methodology, the starting model in the form of lithologies (Fig. 16) is obtained by applying the k-Means method [26] and a comparison of Euclidean distances [31] between the cluster centroid locations and the known lithologies properties in the well (Figs. 14 and 15). This is different from the above-mentioned synthetic example, since there is only one well here and the inversion quality is lower.

The classified and "true" lithologies at the well location are shown in Fig. 17 in which it can be seen that almost all of

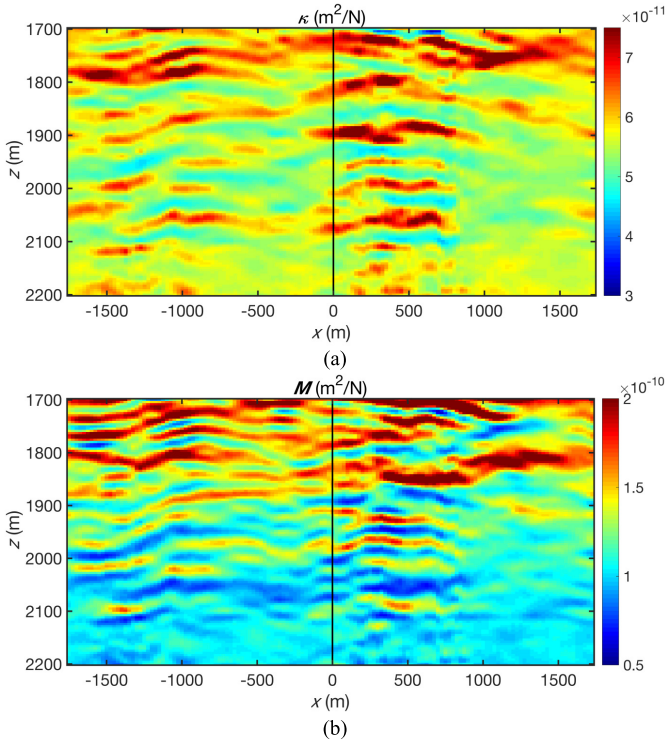

Fig. 13. Inverted rock properties. (a) κ. (b) M. The black line represents the location of the logged well.

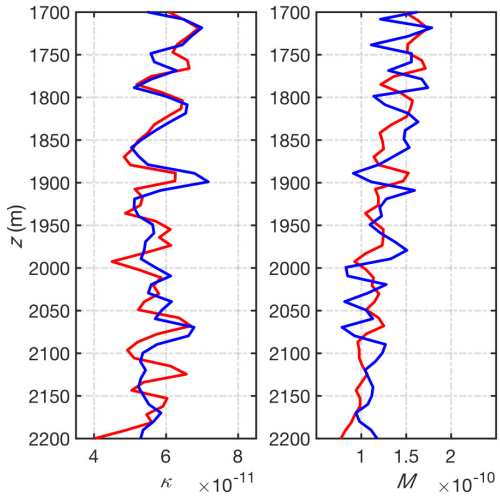

Fig. 14. True (red curves) and inverted (blue curves) rock properties at the logged location (Fig. 13).

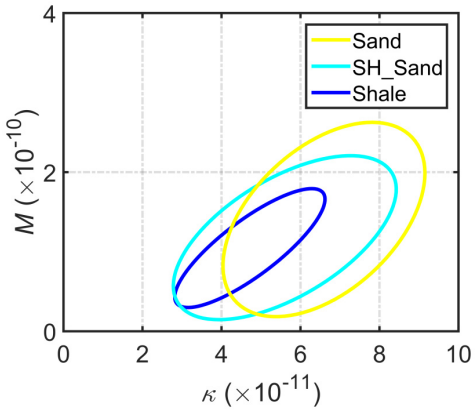

Fig. 15. 90% confidence regions of the bivariate Gaussian likelihood model of lithologies (Sand: sandstone and SH_Sand: shaly sandstone).

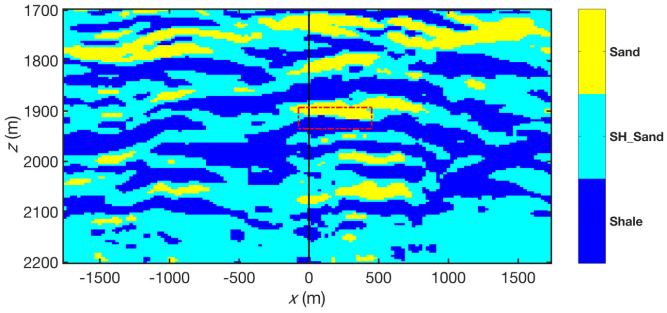

Fig. 16. Starting model in terms of lithologies by k-Means.

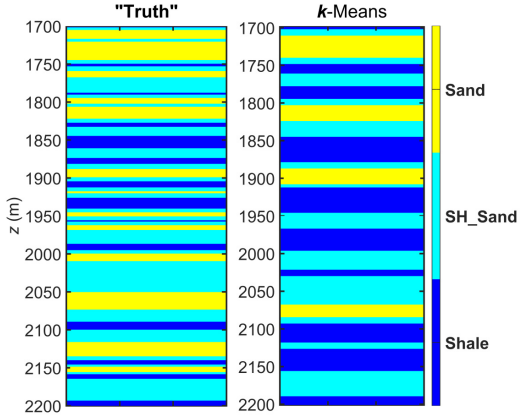

Fig. 17. "Truth" and prediction of k-Means at the well location (black line in Fig. 16).

the sandstone units have been predicted correctly even though the thin shale streaks have been missed due to the low seismic resolution and inversion quality. The "true" lithology is defined based on wireline logging data such as the gamma ray log, instead of cored information.

After applying the proposed GMM-HMRFs in (10) and the profile Markov matrices in Appendix B, the result is shown in Fig. 18.

Compared with the result in Fig. 16, the distributions of lithologies in Fig. 18 are more compact because of the incorporated priors which try to connect and simplify the lithology transitions, therefore reducing the noise in the data. However, there are some "unlikely" transitions, such as sand on top of shale (Fig. 19). (This could happen in many geological settings. But here it is assessed "unlikely," since it does not occur in the cored "truth" well, as shown in Fig. 17.) The reason for this is that small (but not zero) transition probabilities (0.0001) have been assigned in the Markov matrices (Appendix B).

In order to exclude this transition and simulate a typical transition in given reservoirs, such as a water sand not overlying an oil or gas sand because of gravity segregation, Markov matrices are modified as shown in Appendix C. After applying

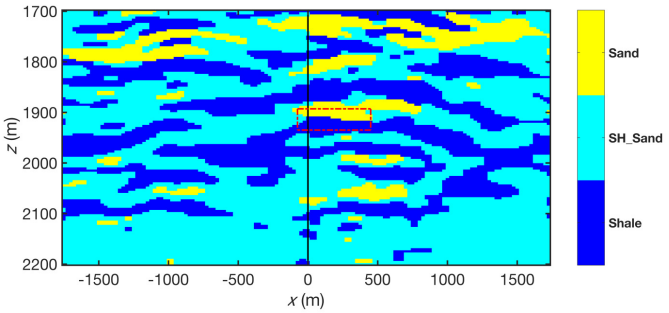

Fig. 18. Classified result of GMM-HMRFs with the Gibbs prior and Markov matrices in Appendix B.

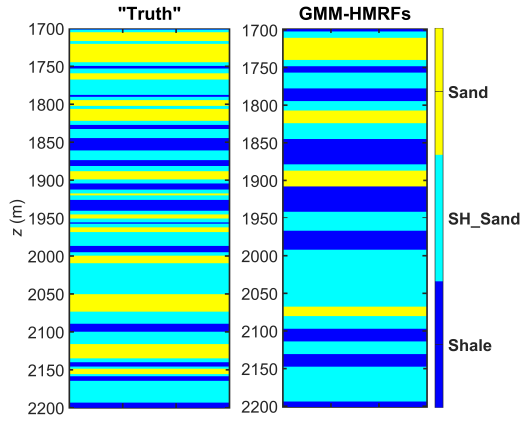

Fig. 19. "Truth" and prediction of GMM-HMRFs at the well location (Fig. 18).

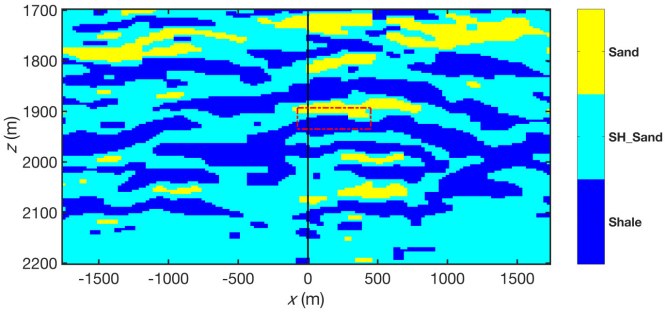

Fig. 20. Classified result of GMM-HMRFs with the Gibbs prior and modified Markov matrices in Appendix C.

these new matrices, the transitions between sand and shale have been removed (Figs. 20 and 21).

VI. Discussion

In this paper, the spatial correlation during the lithological classification process is taken into account through the concept of MRFs, in which the Gibbs prior and the profile Markov matrix are incorporated. In contrast to GMM or k-Means, which do not use the geological spatial prior knowledge, the proposed method of GMM-HMRFs is able to produce better images of categorical variables, and each lithology tends to connect with the same or similar lithology horizontally and vertically based on preferential transitions. Other geostatistical methods such as multiple-point geostatistics [32] cannot be

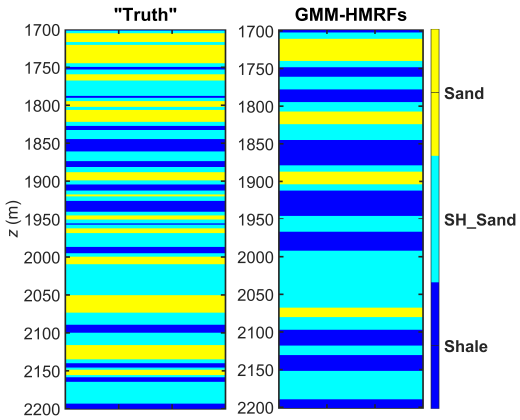

Fig. 21. "Truth" and prediction of GMM-HMRFs at the well location (Fig. 20).

applied for these purposes, since it is not possible to obtain 2-D training images with only a few wells in the subsurface.

A. Input Data Set

The input data for the classification are elastic full-wavefield inversion results [12]. Compared with other inversion methods, this scheme can provide high resolution, since the nonlinear relationship between the rock properties and seismic data has been exploited by utilizing wave-mode conversions and multiple scattering. In contrast to rock properties, such as bulk density and velocities, the compressibility (κ) and shear compliance (M) are used here, because they appear naturally in the elastic wave equation and are more closely related to rock types.

However, the classified result shown in Fig. 12 is not perfect compared with the truth in Fig. 7 especially for SS in the upper part, which has been clustered as VFS. From CMPs 1900 and 2000, the lithology of SS attempts to be continuous in the beginning. However, when moving away from the controlled information of the "drilled" wells, the wrong prediction of VFS emerges and observations from the wells stand out, which is due to errors in the inversion results (Fig. 5) as well as high overlaps in the properties of lithologies (Fig. 6). The same problem happens for SS which has been classified as VFS at the depth 300 m on the left part, even though the starting lithology in the well (CMP = 1900) is correct. Thus, the classification method highly depends on the quality of the input data set and property difference between lithologies, which is also the case for every other classification method. If the inputs cannot provide a good description of the subsurface in terms of rock properties and structures, or if properties of the various lithologies are highly overlapping, perfect prediction of lithologies cannot be expected, even with good geological prior information.

B. Prior Information

The geological prior information that can be incorporated is divided into two groups. One is the Gibbs distribution, which can be obtained from the energy function [see (2) and (3)], and the other one is the transition matrix (Appendixes A–C). Different roles played by these two types of prior information

have been shown in the synthetic example (Figs. 10 and 11), whereby the first one tries to connect lithologies horizontally and vertically and the second one gives preferential transitions between different lithologies, while excluding unlikely transitions (Figs. 20 and 21). The transition matrix can be derived using a general understanding of the depositional environments and the juxtapositions between different lithologies. Application of Walther's law [33] can help in making the construction of these transition matrices easier. As a further research, different scenarios in terms of the Markov matrices could be designed in order to gain more confidence.

C. Number of Lithologies

The number of lithologies to be classified is determined from the cored wells in the cross section and has been maintained constant during the classification process in order to facilitate the prediction problem. However, some lithologies in the middle part of the section may not occur in the wells because of pinch-outs in the layers or 3-D complexities. In the synthetic case, this problem has been avoided, since the well locations can be selected such that all the lithologies occur in the two "wells". In the real cases, this is not possible, and additional geological knowledge, i.e., other fields or well outside the line of section, should be used to address this problem.

D. Markov Matrices

In the 2-D profile Markov transition matrix, the number of matrices is related to the number of states or lithologies in the system. If there are N lithologies, there will be $N(N+1)/2$ matrices which will not be easy to construct, since training images are needed that may not always be available. In the synthetic and real cases presented here, in order to make the matrix construction feasible, values in the transitions are more strongly controlled by the neighbors (Appendixes A–C), and some unlikely transitions can be set to zero as simplified by the transitions between sand and shale in the real case study (red rectangle in Figs. 16, 18, and 20).

E. Starting Model

Since the EM algorithm converges locally, the initial model including the starting lithological section and the parameter sets such as means and covariance matrices in the GMM is important. The histogram analysis helps to estimate the means and covariance matrices in the absence of prior information. According to the criteria of classification, the states should be separated widely from each other in terms of their properties, and at the same time, the intrastate variances need to be as low as possible (Figs. 6 and 15). Other information about these parameters should be brought in, such as a regional or empirical model between the rock properties and lithologies.

Compared with the real case, the inversion quality is better and more "wells" are available in the synthetic example, thus a simple histogram-based method based on the inverted and known properties at the well locations is used in order to provide the initial model (Fig. 8).

In the real case study of Vienna Basin, the inversion quality is low because of problems during the processing phase. Thus, a different approach is adopted in the form of the k-Means to provide the initial model (Fig. 16). The histogram-based method used in the synthetic example has also been tested, but the final result is relatively poor since only one well is available and low-quality means and covariance matrices are provided by the poor inversion at the well location.

VII. Conclusion

In this paper, seismic inversion results have been used as inputs for lithological classification in an approach that circumvents the limitations posed by sparse well locations. The performance of the selected classifier, however, depends highly on the inversion quality. The inversion scheme used here provides high-resolution properties, because it takes the internal multiples and wave-mode conversions also into account.

Geological prior knowledge has been introduced for the classification of reservoir lithologies by applying the MRFs which constrain the vertical and horizontal couplings. Compared with statistical or histogram-based methods, GMM-HMRFs can help make the prediction more geologically reasonable, since lithologies are connected with each other both in the lateral and vertical directions using known preferential probabilities. In this way, a more realistic reservoir architecture can be obtained.

Appendix A
Profile Markov Random Transition Matrix in the Synthetic Example

Adopting the idea as in [8] and [9], the transition matrices of the 2-D MRFs in the synthetic study are as follows:

$$P_{\mathrm{FS,FS}} = \begin{array}{c} \\ \mathrm{FS} \\ \mathrm{VFS} \\ \mathrm{SS} \\ \mathrm{Clay} \end{array} \begin{array}{c} \begin{array}{cccc} \mathrm{FS} & \mathrm{VFS} & \mathrm{SS} & \mathrm{Clay} \end{array} \\ \begin{bmatrix} 0.9997 & 0.0001 & 0.0001 & 0.0001 \\ 0.9997 & 0.0001 & 0.0001 & 0.0001 \\ 0.9997 & 0.0001 & 0.0001 & 0.0001 \\ 0.9997 & 0.0001 & 0.0001 & 0.0001 \end{bmatrix} \end{array} \tag{11}$$

$$P_{\mathrm{FS,VFS}} = \begin{array}{c} \\ \mathrm{FS} \\ \mathrm{VFS} \\ \mathrm{SS} \\ \mathrm{Clay} \end{array} \begin{array}{c} \begin{array}{cccc} \mathrm{FS} & \mathrm{VFS} & \mathrm{SS} & \mathrm{Clay} \end{array} \\ \begin{bmatrix} 0.4998 & 0.5000 & 0.0001 & 0.0001 \\ 0.4998 & 0.5000 & 0.0001 & 0.0001 \\ 0.4998 & 0.5000 & 0.0001 & 0.0001 \\ 0.4998 & 0.5000 & 0.0001 & 0.0001 \end{bmatrix} \end{array} \tag{12}$$

$$P_{\mathrm{FS,SS}} = \begin{array}{c} \\ \mathrm{FS} \\ \mathrm{VFS} \\ \mathrm{SS} \\ \mathrm{Clay} \end{array} \begin{array}{c} \begin{array}{cccc} \mathrm{FS} & \mathrm{VFS} & \mathrm{SS} & \mathrm{Clay} \end{array} \\ \begin{bmatrix} 0.4998 & 0.0001 & 0.5000 & 0.0001 \\ 0.4998 & 0.0001 & 0.5000 & 0.0001 \\ 0.4998 & 0.0001 & 0.5000 & 0.0001 \\ 0.4998 & 0.0001 & 0.5000 & 0.0001 \end{bmatrix} \end{array} \tag{13}$$

$$P_{\mathrm{FS,Clay}} = \begin{array}{c} \\ \mathrm{FS} \\ \mathrm{VFS} \\ \mathrm{SS} \\ \mathrm{Clay} \end{array} \begin{array}{c} \begin{array}{cccc} \mathrm{FS} & \mathrm{VFS} & \mathrm{SS} & \mathrm{Clay} \end{array} \\ \begin{bmatrix} 0.4998 & 0.0001 & 0.0001 & 0.5000 \\ 0.4998 & 0.0001 & 0.0001 & 0.5000 \\ 0.4998 & 0.0001 & 0.0001 & 0.5000 \\ 0.4998 & 0.0001 & 0.0001 & 0.5000 \end{bmatrix} \end{array} \tag{14}$$

$$P_{\mathrm{VFS,VFS}} = \begin{array}{c} \\ \mathrm{FS} \\ \mathrm{VFS} \\ \mathrm{SS} \\ \mathrm{Clay} \end{array} \begin{array}{c} \begin{array}{cccc} \mathrm{FS} & \mathrm{VFS} & \mathrm{SS} & \mathrm{Clay} \end{array} \\ \begin{bmatrix} 0.0001 & 0.9997 & 0.0001 & 0.0001 \\ 0.0001 & 0.9997 & 0.0001 & 0.0001 \\ 0.0001 & 0.9997 & 0.0001 & 0.0001 \\ 0.0001 & 0.9997 & 0.0001 & 0.0001 \end{bmatrix} \end{array} \tag{15}$$

$$P_{\mathrm{VFS,SS}} = \begin{array}{c} \\ \mathrm{FS} \\ \mathrm{VFS} \\ \mathrm{SS} \\ \mathrm{Clay} \end{array} \begin{array}{c} \begin{array}{cccc} \mathrm{FS} & \mathrm{VFS} & \mathrm{SS} & \mathrm{Clay} \end{array} \\ \begin{bmatrix} 0.0001 & 0.4998 & 0.5000 & 0.0001 \\ 0.0001 & 0.4998 & 0.5000 & 0.0001 \\ 0.0001 & 0.4998 & 0.5000 & 0.0001 \\ 0.0001 & 0.4998 & 0.5000 & 0.0001 \end{bmatrix} \end{array} \tag{16}$$

$$P_{\mathrm{VFS,Clay}} = \begin{array}{c} \\ \mathrm{FS} \\ \mathrm{VFS} \\ \mathrm{SS} \\ \mathrm{Clay} \end{array} \begin{array}{c} \begin{array}{cccc} \mathrm{FS} & \mathrm{VFS} & \mathrm{SS} & \mathrm{Clay} \end{array} \\ \begin{bmatrix} 0.0001 & 0.4998 & 0.0001 & 0.5000 \\ 0.0001 & 0.4998 & 0.0001 & 0.5000 \\ 0.0001 & 0.4998 & 0.0001 & 0.5000 \\ 0.0001 & 0.4998 & 0.0001 & 0.5000 \end{bmatrix} \end{array} \tag{17}$$

$$P_{\mathrm{SS,SS}} = \begin{array}{c} \\ \mathrm{FS} \\ \mathrm{VFS} \\ \mathrm{SS} \\ \mathrm{Clay} \end{array} \begin{array}{c} \begin{array}{cccc} \mathrm{FS} & \mathrm{VFS} & \mathrm{SS} & \mathrm{Clay} \end{array} \\ \begin{bmatrix} 0.0001 & 0.0001 & 0.9997 & 0.0001 \\ 0.0001 & 0.0001 & 0.9997 & 0.0001 \\ 0.0001 & 0.0001 & 0.9997 & 0.0001 \\ 0.0001 & 0.0001 & 0.9997 & 0.0001 \end{bmatrix} \end{array} \tag{18}$$

$$P_{\mathrm{SS,Clay}} = \begin{array}{c} \\ \mathrm{FS} \\ \mathrm{VFS} \\ \mathrm{SS} \\ \mathrm{Clay} \end{array} \begin{array}{c} \begin{array}{cccc} \mathrm{FS} & \mathrm{VFS} & \mathrm{SS} & \mathrm{Clay} \end{array} \\ \begin{bmatrix} 0.0001 & 0.0001 & 0.4998 & 0.5000 \\ 0.0001 & 0.0001 & 0.4998 & 0.5000 \\ 0.0001 & 0.0001 & 0.4998 & 0.5000 \\ 0.0001 & 0.0001 & 0.4998 & 0.5000 \end{bmatrix} \end{array} \tag{19}$$

$$P_{\mathrm{Clay,Clay}} = \begin{array}{c} \\ \mathrm{FS} \\ \mathrm{VFS} \\ \mathrm{SS} \\ \mathrm{Clay} \end{array} \begin{array}{c} \begin{array}{cccc} \mathrm{FS} & \mathrm{VFS} & \mathrm{SS} & \mathrm{Clay} \end{array} \\ \begin{bmatrix} 0.0001 & 0.0001 & 0.0001 & 0.9997 \\ 0.0001 & 0.0001 & 0.0001 & 0.9997 \\ 0.0001 & 0.0001 & 0.0001 & 0.9997 \\ 0.0001 & 0.0001 & 0.0001 & 0.9997 \end{bmatrix} \end{array} \tag{20}$$

in which $P_{(:,:)}$ is the transition matrix with horizontal neighbors of different lithologies (FS, VFS, SS, and clay). The vertical transitions between lithologies are controlled by the neighbors which is attributed to the lateral extension of layers.

APPENDIX B
PROFILE MARKOV RANDOM TRANSITION MATRIX IN THE REAL CASE STUDY

The 2-D Markov random matrices in the real case study are as follows:

$$P_{\mathrm{Shale,Shale}} = \begin{array}{c} \\ \mathrm{Shale} \\ \mathrm{SH\_Sand} \\ \mathrm{Sand} \end{array} \begin{array}{c} \begin{array}{ccc} \mathrm{Shale} & \mathrm{SH\_Sand} & \mathrm{Sand} \end{array} \\ \begin{bmatrix} 0.9998 & 0.0001 & 0.0001 \\ 0.9998 & 0.0001 & 0.0001 \\ 0.9998 & 0.0001 & 0.0001 \end{bmatrix} \end{array} \tag{21}$$

$$P_{\mathrm{Shale,SH\_Sand}} = \begin{array}{c} \\ \mathrm{Shale} \\ \mathrm{SH\_Sand} \\ \mathrm{Sand} \end{array} \begin{array}{c} \begin{array}{ccc} \mathrm{Shale} & \mathrm{SH\_Sand} & \mathrm{Sand} \end{array} \\ \begin{bmatrix} 0.4999 & 0.5000 & 0.0001 \\ 0.4999 & 0.5000 & 0.0001 \\ 0.4999 & 0.5000 & 0.0001 \end{bmatrix} \end{array} \tag{22}$$

$$P_{\mathrm{Shale,Sand}} = \begin{array}{c} \\ \mathrm{Shale} \\ \mathrm{SH\_Sand} \\ \mathrm{Sand} \end{array} \begin{array}{c} \begin{array}{ccc} \mathrm{Shale} & \mathrm{SH\_Sand} & \mathrm{Sand} \end{array} \\ \begin{bmatrix} 0.4999 & 0.0001 & 0.5000 \\ 0.4999 & 0.0001 & 0.5000 \\ 0.4999 & 0.0001 & 0.5000 \end{bmatrix} \end{array} \tag{23}$$

$$P_{\mathrm{SH\_Sand,SH\_Sand}} = \begin{array}{c} \\ \mathrm{Shale} \\ \mathrm{SH\_Sand} \\ \mathrm{Sand} \end{array} \begin{array}{c} \begin{array}{ccc} \mathrm{Shale} & \mathrm{SH\_Sand} & \mathrm{Sand} \end{array} \\ \begin{bmatrix} 0.0001 & 0.9998 & 0.0001 \\ 0.0001 & 0.9998 & 0.0001 \\ 0.0001 & 0.9998 & 0.0001 \end{bmatrix} \end{array} \tag{24}$$

$$P_{\mathrm{SH\_Sand,Sand}} = \begin{array}{c} \\ \mathrm{Shale} \\ \mathrm{SH\_Sand} \\ \mathrm{Sand} \end{array} \begin{array}{c} \begin{array}{ccc} \mathrm{Shale} & \mathrm{SH\_Sand} & \mathrm{Sand} \end{array} \\ \begin{bmatrix} 0.0001 & 0.4999 & 0.5000 \\ 0.0001 & 0.4999 & 0.5000 \\ 0.0001 & 0.4999 & 0.5000 \end{bmatrix} \end{array} \tag{25}$$

$$P_{\mathrm{Sand,Sand}} = \begin{array}{c} \\ \mathrm{Shale} \\ \mathrm{SH\_Sand} \\ \mathrm{Sand} \end{array} \begin{array}{c} \begin{array}{ccc} \mathrm{Shale} & \mathrm{SH\_Sand} & \mathrm{Sand} \end{array} \\ \begin{bmatrix} 0.0001 & 0.0001 & 0.9998 \\ 0.0001 & 0.0001 & 0.9998 \\ 0.0001 & 0.0001 & 0.9998 \end{bmatrix} \end{array} \tag{26}$$

APPENDIX C
MODIFIED PROFILE MARKOV RANDOM TRANSITION MATRIX IN THE REAL CASE STUDY

The 2-D modified Markov random matrices of the real case study in order to simulate the unlikely transitions in a separated reservoir are as follows:

$$P_{\mathrm{Shale,Shale}} = \begin{array}{c} \\ \mathrm{Shale} \\ \mathrm{SH\_Sand} \\ \mathrm{Sand} \end{array} \begin{array}{c} \begin{array}{ccc} \mathrm{Shale} & \mathrm{SH\_Sand} & \mathrm{Sand} \end{array} \\ \begin{bmatrix} 0.9999 & 0.0001 & 0 \\ 0.9998 & 0.0001 & 0.0001 \\ 0 & 0.5000 & 0.5000 \end{bmatrix} \end{array} \tag{27}$$

$$P_{\mathrm{Shale,SH\_Sand}} = \begin{array}{c} \\ \mathrm{Shale} \\ \mathrm{SH\_Sand} \\ \mathrm{Sand} \end{array} \begin{array}{c} \begin{array}{ccc} \mathrm{Shale} & \mathrm{SH\_Sand} & \mathrm{Sand} \end{array} \\ \begin{bmatrix} 0.5000 & 0.5000 & 0 \\ 0.4999 & 0.5000 & 0.0001 \\ 0 & 0.9999 & 0.0001 \end{bmatrix} \end{array} \tag{28}$$

$$P_{\mathrm{Shale,Sand}} = \begin{array}{c} \\ \mathrm{Shale} \\ \mathrm{SH\_Sand} \\ \mathrm{Sand} \end{array} \begin{array}{c} \begin{array}{ccc} \mathrm{Shale} & \mathrm{SH\_Sand} & \mathrm{Sand} \end{array} \\ \begin{bmatrix} 0.9999 & 0.0001 & 0 \\ 0.4999 & 0.0001 & 0.5000 \\ 0 & 0.0001 & 0.9999 \end{bmatrix} \end{array} \tag{29}$$

$$P_{\text{SH\_Sand,SH\_Sand}} = \begin{array}{c} \\ \text{Shale} \\ \text{SH\_Sand} \\ \text{Sand} \end{array} \begin{array}{c} \begin{array}{ccc} \text{Shale} & \text{SH\_Sand} & \text{Sand} \end{array} \\ \begin{bmatrix} 0.0001 & 0.9999 & 0 \\ 0.0001 & 0.9998 & 0.0001 \\ 0 & 0.9999 & 0.0001 \end{bmatrix} \end{array} \tag{30}$$

$$P_{\text{SH\_Sand,Sand}} = \begin{array}{c} \\ \text{Shale} \\ \text{SH\_Sand} \\ \text{Sand} \end{array} \begin{array}{c} \begin{array}{ccc} \text{Shale} & \text{SH\_Sand} & \text{Sand} \end{array} \\ \begin{bmatrix} 0.0001 & 0.9999 & 0 \\ 0.0001 & 0.4999 & 0.5000 \\ 0 & 0.5000 & 0.5000 \end{bmatrix} \end{array} \tag{31}$$

$$P_{\text{Sand,Sand}} = \begin{array}{c} \\ \text{Shale} \\ \text{SH\_Sand} \\ \text{Sand} \end{array} \begin{array}{c} \begin{array}{ccc} \text{Shale} & \text{SH\_Sand} & \text{Sand} \end{array} \\ \begin{bmatrix} 0.5000 & 0.5000 & 0 \\ 0.0001 & 0.0001 & 0.9998 \\ 0 & 0.0001 & 0.9999 \end{bmatrix} \end{array} \tag{32}$$

ACKNOWLEDGMENT

The authors would like to thank OMV Exploration & Production for permission to publish this data. The inversion of seismic data of the real case study is done with the help of P. Doulgeris of Delft Inversion, Delft, The Netherlands.

REFERENCES

[1] A. L. Larsen, M. Ulvmoen, H. Omre, and A. Buland, "Bayesian lithology/fluid prediction and simulation on the basis of a Markov-chain prior model," *Geophysics*, vol. 71, no. 5, pp. R69–R78, Sep. 2006.

[2] T. Mukerji, A. Jørstad, P. Avseth, G. Mavko, and J. R. Granli, "Mapping lithofacies and pore-fluid probabilities in a North Sea reservoir: Seismic inversions and statistical rock physics," *Geophysics*, vol. 66, no. 4, pp. 988–1001, Jul. 2001.

[3] R. T. Houck, "Quantifying the uncertainty in an AVO interpretation," *Geophysics*, vol. 67, no. 1, pp. 117–125, Jan. 2002.

[4] A. Buland and H. Omre, "Bayesian linearized AVO inversion," *Geophysics*, vol. 68, no. 1, pp. 185–198, Jan. 2003.

[5] A. Buland, O. Kolbjørnsen, R. Hauge, Ø. Skjæveland, and K. Duffaut, "Bayesian lithology and fluid prediction from seismic prestack data," *Geophysics*, vol. 73, no. 3, pp. C13–C21, May 2008.

[6] J. Eidsvik, T. Mukerji, and P. Switzer, "Estimation of geological attributes from a well log: An application of hidden Markov chains," *Math. Geol.*, vol. 36, no. 3, pp. 379–397, Apr. 2004.

[7] M. Ulvmoen and H. Hammer, "Bayesian lithology/fluid inversion—Comparison of two algorithms," *Comput. Geosci.*, vol. 14, no. 2, pp. 357–367, Mar. 2010.

[8] M. Ulvmoen and H. Omre, "Improved resolution in Bayesian lithology/fluid inversion from prestack seismic data and well observations: Part 1—Methodology," *Geophysics*, vol. 75, no. 2, pp. R21–R35, Mar. 2010.

[9] M. Ulvmoen, H. Omre, and A. Buland, "Improved resolution in Bayesian lithology/fluid inversion from prestack seismic data and well observations: Part 2—Real case study," *Geophysics*, vol. 75, no. 2, pp. B73–B82, Mar. 2010.

[10] H. Hammer, O. Kolbjørnsen, H. Tjelmeland, and A. Buland, "Lithology and fluid prediction from prestack seismic data using a Bayesian model with Markov process prior," *Geophys. Prospecting*, vol. 60, no. 3, pp. 500–515, May 2012.

[11] M. Bosch, C. Carvajal, J. Rodrigues, A. Torres, M. Aldana, and J. Sierra, "Petrophysical seismic inversion conditioned to well-log data: Methods and application to a gas reservoir," *Geophysics*, vol. 74, no. 2, pp. O01–O15, Mar. 2009.

[12] A. Gisolf, R. Huis in't Veld, P. Haffinger, C. Hanitzsch, P. Doulgeris, and P. C. H. Veeken, "Non-linear full wavefield inversion applied to carboniferous reservoirs in the wingate gas field (SNS, Offshore UK)," in *Proc. 76th EAGE Annu. Meeting*, 2014.

[13] D. V. Lindberg and D. Grana, "Petro-elastic log-facies classification using the expectationâŁ"maximization algorithm and hidden Markov models," *Math. Geosci.*, vol. 47, no. 6, pp. 719–752, Aug. 2015.

[14] P. Avseth, T. Mukerji, and G. Mavko, *Quantitative Seismic Interpretation: Applying Rock Physics Tools to Reduce Interpretation Risk*. Cambridge, U.K.: Cambridge Univ. Press, 2005.

[15] M. A. Shahrabi, H. Hashemi, and M. K. Hafizi, "Application of mixture of Gaussian clustering on joint facies interpretation of seismic and magnetotelluric sections," *Pure Appl. Geophys.*, vol. 173, no. 2, pp. 623–636, Feb. 2016.

[16] E. Ising, "Beitrag zur Theorie des Ferromagnetismus," *Zeitschrift Phys. A, Hadrons Nuclei*, vol. 31, no. 1, pp. 253–258, Feb. 1925.

[17] J. Besag, "Spatial interaction and the statistical analysis of lattice systems," *J. Roy. Statist. Soc. B, Methodol.*, vol. 36, no. 2, pp. 192–236, 1974.

[18] G. Winkler, *Image Analysis, Random Fields and Markov Chain Monte Carlo Methods: A Mathematical Introduction*. Heidelberg, Germany: Springer, 2003.

[19] H. Wang, J. F. Wellmann, Z. Li, X. Wang, and R. Y. Liang, "A segmentation approach for stochastic geological modelling using hidden Markov random field," *Math. Geosci.*, vol. 49, no. 2, pp. 145–177, Feb. 2017.

[20] L. Rabiner, "A tutorial on hidden Markov models and selected applications in speech recognition," *Proc. IEEE*, vol. 77, no. 2, pp. 257–286, Feb. 1989.

[21] Q. Wang. (Dec. 2012). "GMM-based hidden Markov random field for color image and 3D volume segmentation." [Online]. Available: https://arxiv.org/abs/1212.4527

[22] Y. Zhang, M. Brady, and S. Smith, "Segmentation of brain MR images through a hidden Markov random field model and the expectation-maximization algorithm," *IEEE Trans. Med. Imag.*, vol. 20, no. 1, pp. 45–57, Jan. 2001.

[23] A. Elfeki and M. Dekking, "A Markov chain model for subsurface characterization: Theory and applications," *Math. Geol.*, vol. 33, no. 5, pp. 569–589, Jul. 2001.

[24] R. H. Feng, S. M. Luthi, A. Gisolf, and S. Sharma, "Obtaining a high-resolution geological and petrophysical model from the results of reservoir-orientated elastic wave-equation-based seismic inversion," *Petroleum Geosci.*, vol. 23, no. 3, pp. 376–385, Feb. 2017.

[25] D. Tetyukhina, S. M. Luthi, and D. Gisolf, "Acoustic nonlinear full-waveform inversion on an outcrop-based detailed geological and petrophysical model (Book Cliffs, Utah)," *AAPG Bull.*, vol. 98, no. 1, pp. 119–134, Jan. 2014.

[26] G. A. F. Seber, *Multivariate Observations*. New York, NY, USA: Wiley, 1984.

[27] B. W. Matthews, "Comparison of the predicted and observed secondary structure of T4 phage lysozyme," *Biochimica Biophysica Acta*, vol. 405, no. 2, pp. 442–451, Oct. 1975.

[28] D. Grana and E. D. Rossa, "Probabilistic petrophysical-properties estimation integrating statistical rock physics with seismic inversion," *Geophysics*, vol. 75, no. 3, pp. O21–O37, May 2010.

[29] H. B. Zhang, Q. Guo, L. F. Liang, C. H. Cao, and Z. P. Shang, "A nonlinear method for multiparameter inversion of pre-stack seismic data based on anisotropic Markov random field," *Geophys. Prospecting*, vol. 66, no. 3, pp. 461–477, Mar. 2018.

[30] R. H. Feng, S. M. Luthi, and A. Gisolf, "Simulating reservoir lithologies by an actively conditioned Markov chain model," *J. Geophys. Eng.*, vol. 15, no. 3, pp. 800–815, Jun. 2018.

[31] M. M. Deza and E. Deza, *Encyclopedia of Distance*. Heidelberg, Germany: Springer, 2009.

[32] S. Strebelle, "Conditional simulation of complex geological structures using multiple-point statistics," *Math. Geol.*, vol. 34, no. 1, pp. 1–21, Jan. 2002.

[33] G. V. Middleton, "Johannes Walther's law of the correlation of facies," *GSA Bull.*, vol. 84, no. 3, pp. 979–988, Mar. 1973.

Runhai Feng received the B.Sc. degree in prospecting engineering from the China University of Geosciences, Wuhan, China, and the M.Sc. degree in geophysics from Nanjing University, Nanjing, China. He is currently pursuing the Ph.D. degree with the Delft University of Technology, Delft, The Netherlands.

As a member of the Delphi Consortium, Delft, he is involved in the integration of geological prior information in reservoir characterization.

Stefan M. Luthi received the M.Sc. and Ph.D. degrees from the Swiss Federal Institute of Technology, ETH Zürich, Zürich, Switzerland.

He is currently an Emeritus Professor of reservoir geology with the Delft University of Technology, Delft, The Netherlands. As a Senior Technical Advisor with Schlumberger, Houston, TX, USA, he was with the hydrocarbon industry for over 30 years.

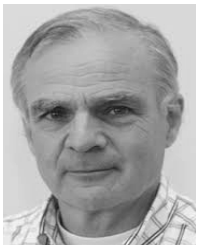

Dries Gisolf received the M.Sc. degree in applied physics from the Delft University of Technology, Delft, The Netherlands, in 1971, and the Ph.D. degree from Utrecht University, Utrecht, The Netherlands, in 1975.

After retiring as a Professor from the Delft University of Technology, he co-founded the service company Delft Inversion, Delft.

Erika Angerer received the Engineering degree (Dipl.Ing.) in applied geophysics from the University of Mining Leoben, Leoben, Austria, and the Ph.D. degree in geophysics from The University of Edinburgh, Edinburgh, U.K.

She is currently with OMV Exploration & Production, Vienna, Austria, as a Reservoir Geophysicist, where she is involved in development and enhanced oil recovery in mature fields.